

The Hubble Tension Bites the Dust: Sensitivity of the Hubble Constant Determination to Cepheid Color Calibration

EDVARD MÖRTSELL,¹ ARIEL GOOBAR,¹ JOEL JOHANSSON,¹ AND SUHAIL DHAWAN²

¹*Oskar Klein Centre, Department of Physics, Stockholm University
Albanova University Center
106 91 Stockholm, Sweden*

²*Institute of Astronomy
University of Cambridge Madingley Road
Cambridge CB3 0HA
United Kingdom*

ABSTRACT

Motivated by the large observed diversity in the properties of extra-galactic extinction by dust, we re-analyse the Cepheid calibration used to infer the local value of the Hubble constant, H_0 , from Type Ia supernovae. Unlike the SH0ES team, we do not enforce a universal color-luminosity relation to correct the near-IR Cepheid magnitudes. Instead, we focus on a data driven method, where the measured colors of the Cepheids are used to derive a color-luminosity relation for each galaxy individually. We present two different analyses, one based on Wesenheit magnitudes, a common practice in the field that attempts to combine corrections from both extinction and variations in intrinsic colors, resulting in $H_0 = 66.9 \pm 2.5$ km/s/Mpc, in agreement with the Planck value. In the second approach, we calibrate using color excesses with respect to derived average intrinsic colors, yielding $H_0 = 71.8 \pm 1.6$ km/s/Mpc, a 2.7σ tension with the value inferred from the cosmic microwave background.

Hence, we argue that systematic uncertainties related to the choice of Cepheid color-luminosity calibration method currently inhibits us from measuring H_0 to the precision required to claim a substantial tension with Planck data.

Keywords: Cepheid distance (217), Hubble constant (758), Type Ia supernovae (1728), Interstellar dust extinction (837)

1. INTRODUCTION

As is well known, there is a tension between the value of the Hubble constant as inferred from small and large distance measurements, most significantly between the values inferred from Type Ia supernova (SNIa) distances to redshifts $z \sim 0.1$ calibrated by Cepheid observations, as measured by the SH0ES team, and the distance to the cosmic microwave background (CMB) decoupling surface at $z \sim 1090$, as measured by the Planck satellite. The former yields $H_0 = 73.2 \pm 1.3$ (in units of km/s/Mpc used from now on) (Riess et al. 2021) and the latter $H_0 = 67.4 \pm 0.5$ (Aghanim et al. 2020); a 4.1σ tension.

The tension between other measurements is not as significant: Calibrating the absolute SNIa magnitude using the tip of the red giant branch (TRGB) observations gives $H_0 = 69.6 \pm 1.6$ (Freedman et al. 2019), right between the Cepheid calibrated SNIa and the CMB inferred values.

Another local estimate of the expansion rate of the Universe is derived from the amplitude of the gravitational wave signal GW170817, the merger of a binary neutron-star system located to the galaxy NGC 4993 at $z = 0.010$ through the electromagnetic counterpart, AT2017gfo, yielding a Hubble constant with relatively large uncertainties of $H_0 = 70.0^{+12.0}_{-8.0}$ (Abbott et al. 2017).

A different route involves gravitational lensing. Time delays in the TDCOSMO sample of seven lensed quasars yield $H_0 = 74.5^{+5.6}_{-6.1}$ (Birrer et al. 2020). Constraining

the galaxy lens mass profiles, using kinematics observations of an independent set of gravitational lenses in the Sloan Lens ACS sample (SLACS), lowers the value to $H_0 = 67.4^{+4.1}_{-3.2}$, assuming that the TDCOSMO and SLACS galaxies are drawn from the same parent population. These results are illustrated in Figure 1, from which is evident that only the Cepheid calibrated SNIa distance scale from SH0ES is in definite tension with the CMB inferred distance.

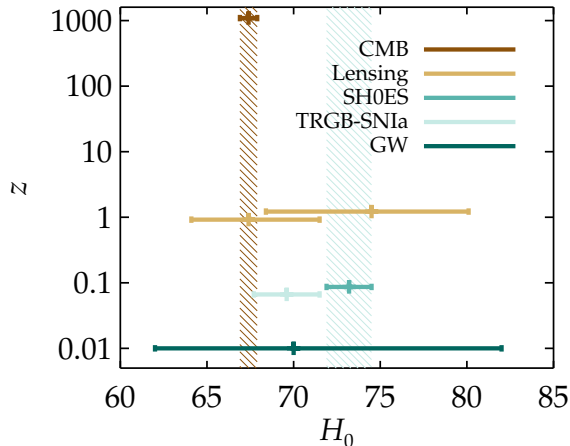


Figure 1. The Hubble constant as inferred from distances measured to the CMB, strongly lensed quasars, SNIa calibrated with Cepheids (SH0ES) and the TRGB, and the gravitational wave signal GW170817. The redshift corresponds to the mean redshift of the distances employed in the method, slightly shifted where needed to avoid overlap. The major tension is between the values inferred from Cepheid calibrated SNIa by the SH0ES team and CMB observations.

The value inferred from the CMB depends on the entire expansion history of the Universe, whereas the SNIa measurement only depends on the local expansion rate it sets out to measure. On the other hand, the inference from SNe Ia depends on a combination of a larger number of astrophysical probes. Therefore, attempts to modify the CMB inferred H_0 usually rely on modifications of the cosmological model, whereas the SNIa value is usually studied with emphasis on possible systematic effects concerning the local distance measurements.

At least in principle, the CMB value can be increased by various departures from the concordance cosmological constant and cold dark matter, Λ CDM model, see e.g. Mörtzell & Dhawan (2018); Knox & Millea (2020). Options include decreasing the physical size of the sound horizon used to measure the distance to $z = 1090$. This can be accomplished by adding sources of energy

present before CMB photon decoupling, e.g., new thermal relativistic species or early dark energy, or by reducing the sound speed. However, such modifications are severely constrained when taking the full CMB power spectrum into account. Attempts to shift the CMB value also involve changing the expansion history at redshifts $z < 1090$, with modest success since the expansion rate is tightly constrained by SNIa and baryonic acoustic oscillation (BAO) observations.

Given that the proposals mentioned above require substantial modifications of the current concordance cosmological model, and still fail in relieving the full tension, we investigate the Cepheid-SNIa value and its uncertainties, see also Follin & Knox (2018); Efstathiou (2020). In particular, we concentrate on dust extinction, affecting all astronomical observations in the optical and near infrared (NIR) regime. We focus on a very specific assumption made by the SH0ES team throughout their series of publications, namely that there is a *universal* reddening law in all galaxies.

2. REVISITING DUST EXTINCTION CORRECTIONS

In spite of the critical importance for precision cosmology, the current understanding of light attenuation in the interstellar medium (ISM) of galaxies remains very limited. In comparison, the Milky Way (MW) ISM has been studied in great detail, including the properties of dust grains responsible for dimming of light (see Draine 2003, for a review). In particular, several MW reddening laws have been devised, among these Cardelli et al. (1989) (CCM), O’Donnell (1994) and Fitzpatrick (1999) (F99). They have in common the use of a single parameter, the total to selective extinction coefficient, R_V^{BV} , as a proxy for the grain composition and size distribution, where the attenuation in the optical V-band relates to the color excess $E(B - V) \equiv A_B - A_V$ as $A_V = R_V^{BV} E(B - V)$, here referred to as the “CCM-relationship”. Low values of R_V^{BV} indicate a steep wavelength dependence, while large R_V^{BV} correspond to gray extinction.

While an average $\langle R_V^{BV} \rangle = 3.1$ for the MW is found in most studies, significant variations are found in individual lines of sight in the galaxy, ranging from $R_V^{BV} \approx 2$ in some diffuse sight lines, to $R_V^{BV} \approx 6$ in dense molecular clouds (Fitzpatrick 1999). The diversity in the MW has been confirmed by Nataf et al. (2016), who find significantly lower values of R_V^{BV} in the Galactic bulge. Moving the scope outside the MW, a study by Gordon et al. (2003) of the extinction in the Magellanic Clouds found that a small number of LMC extinction curves are consistent with the CCM relation-

ship, but the majority of the LMC and all the SMC curves are not. Fausnaugh et al. (2015) report a gray extinction law for NGC 4258 in the line of sight of the Cepheids, $R_V^{BV} \sim 4.9$, although they caution that this could be the result of unresolved systematics. For more distant galaxies, observed SNIa colors highlight the observed diversity in extinction properties, ranging from $R_V^{BV} \sim 1$ to values consistent with the MW average (see Krisciunas et al. 2006; Nobili & Goobar 2008; Goobar et al. 2014; Amanullah et al. 2014, 2015; Burns et al. 2018, and references therein). For the SNe Ia in the Hubble flow, color corrections are based on the SALT2 lightcurve fitter (Guy et al. 2007), which again differ from the CCM parameterization, but are most consistent with values of $R_V^{BV} \sim 2.5$ (see e.g., Biswas et al. 2021, and references therein), although dust extinction differences between host galaxy environments has been suggested as an explanation for a systematic "mass step" in the derived distances (Brout & Scolnic 2021; Johansson et al. 2021).

To minimize the impact from extinction correction uncertainties, the SH0ES team use flux measurements in the NIR H-band, centered at $1.6 \mu m$, where extinction by dust, gauged using the observed color $V - I$, is significantly smaller. Adopting the CCM-like relationship from F99 and the extinction correction $A_H = R_H^{VI} E(V - I)$, the value corresponding to the MW average is $R_H^{VI} \sim 0.4$. However, there is no theoretical, nor any empirical studies of extinction suggesting that a *universal* value of R_H^{VI} can be assumed. On the contrary, a recent study by Fitzpatrick et al. (2019) finds considerable variations between lines of sight for the extinction curves in the NIR in the Milky-Way. Based on a parameterization fitting extinction laws from ultraviolet to NIR for 72 well-measured stars, a very wide range in R_H^{VI} can be inferred, as shown in Figure 2. Hence, assuming a narrow range in R_H^{VI} for the anchor and Cepheid hosts is not warranted by current observations. In this paper, we investigate to what degree relaxing this assumption affects the inferred value of H_0 and its corresponding uncertainties.

3. DIFFERENCE IN METHODOLOGY

The local distance ladder uses the difference between Cepheid magnitudes in SNIa hosts and anchor galaxies. Therefore, it is relatively insensitive to changes in the *global* properties of the extinction law. In Riess et al. (2016), a global change of the parameter R_W parameterizing a Cepheid color-luminosity (C-L) correction with respect to the observed color $R_W (V - I)$ of $R_W = 0.39 \rightarrow 0.35$ changed the Hubble constant by $\delta H_0 \sim 0.5$. When multiplied with the observed color $V - I$, the param-

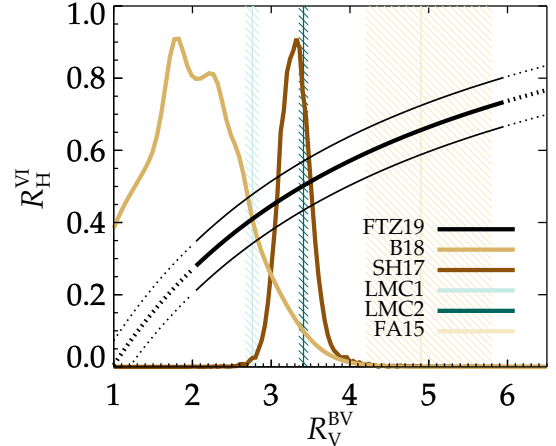


Figure 2. R_H^{VI} vs R_V^{BV} relation and 1σ scatter from the extinction law derived by Fitzpatrick et al. (2019) (FTZ19), extrapolated to $R_V^{BV} > 6$ and $R_V^{BV} < 2$. Such low values have been inferred from SNIa colors (Burns et al. 2018, B18). Also shown are derived R_V^{BV} values from a MW stellar sample in Schlafly et al. (2017) (SH17), two samples in the LMC (Gordon et al. 2003, LMC1 and LMC2) and in the water mega-maser anchor NGC 4258 (Fausnaugh et al. 2015, FA15).

ter R_W is argued to also partly correct for an intrinsic Cepheid C-L relation.

In Follin & Knox (2018), a slightly different C-L correction with respect to an estimated color excess of $R_E \hat{E}(V - I)$ was employed, where $\hat{E}(V - I) \equiv (V - I) - \langle V - I \rangle_0$ with $\langle V - I \rangle_0$ an estimate of the mean intrinsic Cepheid color. Here, R_E is interpreted as the dust total to selective extinction ratio, R_H^{VI} . Imposing a prior of $R_E = 0.39 \pm 0.1$, a value of $H_0 = 73.3 \pm 1.7$ was derived when allowing R_E to vary between galaxies, in good agreement with $H_0 = 73.2 \pm 1.3$ from Riess et al. (2021). At face value, this result seems to suggest that the method used for calibrating the C-L relation and/or the possibility of varying this calibration between galaxies have a small impact on the inferred Hubble constant.

As argued below, regardless of whether calibrating with respect to the observed color or an estimated color excess, the correction should apply for both dust extinction and the intrinsic Cepheid C-L relation. Since both contributions are uncertain at NIR wavelengths, and at least dust extinction properties are known to vary between galaxies, we investigate the effect of allowing for R_W and R_E to do the same. Given the lack of solid independent constraints on R_E , we employ less restrictive priors than Follin & Knox (2018). Any systematic difference in dust properties or the intrinsic C-L between SNIa hosts and anchor galaxies will shift the inferred

value of H_0 . We will show that such a difference is supported by the Cepheid and SNIa data.

4. METHOD AND DATA

The apparent magnitude of a source at redshift z with absolute magnitude M is given by

$$m = 5 \log D(z) + M + 25, \quad (1)$$

where $D(z)$ is the luminosity distance in units of Mpc. By combining observed magnitudes of Cepheids in SNIa host and anchor galaxies, $m_{\text{CepH}}^{\text{host}}$ and $m_{\text{CepH}}^{\text{anch}}$ with SNIa magnitudes in host galaxies and in the Hubble flow, $m_{\text{SN}}^{\text{host}}$ and $m_{\text{SN}}^{\text{flow}}$, we can derive

$$5 \log H_0 = 5 \log r(z) - 5 \log D^{\text{anch}} + \Delta m_{\text{SN}} - \Delta m_{\text{CepH}}, \quad (2)$$

where $r(z) \equiv H_0 D(z)$ can be approximated by $r(z) \approx cz$ in the close Hubble flow and we have defined

$$\Delta m_{\text{SN}} \equiv m_{\text{SN}}^{\text{host}} - m_{\text{SN}}^{\text{flow}}, \quad (3)$$

$$\Delta m_{\text{CepH}} \equiv m_{\text{CepH}}^{\text{host}} - m_{\text{CepH}}^{\text{anch}}. \quad (4)$$

Apart from getting the SNIa redshifts and anchor distances right, we thus need to make sure there are no systematic offsets in the Cepheid and SNIa magnitudes between host, anchor and cosmic flow galaxies. Ignoring the weak cosmology dependence of $r(z)$ (Dhawan et al. 2020), the inferred value of H_0 will decrease (increase) if we:

1. Increase (decrease) the independent anchor distances, D^{anch} .
2. Decrease (increase) Δm_{SN} .
3. Increase (decrease) Δm_{CepH} .

Here, we focus on option 3. With regards to option 2, Δm_{SN} will increase if SNIa in Cepheid host galaxies are systematically made brighter than in the Hubble flow, e.g., if there is additional dust extinction not accounted for in the host galaxies, or if the effect that SNIa in high mass hosts are systematically brighter than in low mass galaxies, such as Cepheid hosts, have been underestimated (see Rigault et al. 2020, and references therein).

In terms of option 3, if there is additional dust extinction not accounted for in the anchor galaxies, or if we have over-corrected for dust extinction in the host galaxies, the inferred value of H_0 will decrease, and vice versa. The fractional shift in the Hubble constant is

$$\frac{\delta H_0}{H_0} = \frac{\delta r(z)}{r(z)} - \frac{\delta D^{\text{anch}}}{D^{\text{anch}}} + \frac{\ln 10}{5} [\delta(\Delta m_{\text{SN}}) - \delta(\Delta m_{\text{CepH}})], \quad (5)$$

and a lower limit to the precision in H_0 is set by the precision of the anchor distance measurements. Shifting $\delta(\Delta m_{\text{CepH}}) = \pm 0.1$ will shift the Hubble constant by $\delta H_0 \mp 4.6\%$.

4.1. Cepheid calibration

We use the Hubble Space Telescope (HST) flux in the NIR filter (H = F160W) band, color calibrated using optical (V = F555W and I = F814W) data, to derive Wesenheit magnitudes

$$m_{\text{H}}^{\text{W}} \equiv m_{\text{H}} - R_{\text{W}}(V-I) = m_{\text{H}} - R_{\text{W}} E(V-I) - R_{\text{W}}(V-I)_0, \quad (6)$$

where the color excess $E(V-I) \equiv A_{\text{V}} - A_{\text{I}} = (V-I) - (V-I)_0$, with $(V-I)_0$ the intrinsic Cepheid color. In the last step, we see that m_{H}^{W} is corrected both for dust extinction, identifying the first R_{W} with the total to selective extinction ratio $R_{\text{H}}^{\text{VI}} \equiv A_{\text{H}}/(A_{\text{V}} - A_{\text{I}})$, and for a possible intrinsic C-L relation, identifying the second R_{W} with $\beta_{\text{H}}^{\text{VI}}$, as parameterized in e.g. Madore (1982) and Madore et al. (2017). The term $\beta_{\text{H}}^{\text{VI}}(V-I)_0$ corresponds to the intrinsic magnitude-color relation at a fixed Cepheid period, whereas the correlation between the intrinsic color with period is included in the period-luminosity (P-L) calibration parameterized by b_{W} in equation 9 below. As an alternative approach, also employed in Follin & Knox (2018), we calibrate the C-L relation using

$$m_{\text{H}}^{\text{W}} \equiv m_{\text{H}} - R_{\text{E}} \hat{E}(V-I). \quad (7)$$

Here, $\hat{E}(V-I)$ represents a proxy for the color excess obtained by subtracting an estimate of the mean intrinsic colors, $\langle V-I \rangle_0$ from the observed colors¹,

$$\hat{E}(V-I) \equiv (V-I) - \langle V-I \rangle_0. \quad (8)$$

The estimated color excess $\hat{E}(V-I)$ also represents a combination of dust extinction and intrinsic color, since the mean intrinsic colors, $\langle V-I \rangle_0$ does not take into account individual variations in Cepheid temperature along the width of the Cepheid instability strip, see e.g. Pejcha & Kochanek (2012).

Using multi wavelength data, one can in principle attempt to distinguish the contribution from dust and intrinsic color variations, see e.g. Pejcha & Kochanek (2012); Madore et al. (2017) and calibrate them separately. In the following, we will follow standard practice and assume that R_{W} and R_{E} effectively corrects both for

¹ Note that if $\langle V-I \rangle_0$ is assumed to depend on the Cepheid period, the fitted b_{W} parameterizing the P-L relation will shift accordingly.

dust and intrinsic color variations, but remain agnostic whether this is most effectively done using the Wesenheit calibration using observed colors or with respect to estimated color excesses. Taking an empirical approach, in both cases, we will fit for the values of R_W and R_E that minimize the scatter in m_H^W .

We model the Wesenheit magnitude of the j th Cepheid in the i th SNIa host as

$$m_{H,i,j}^W = \mu_i + M_H^W + b_W[P]_{i,j} + Z_W[M/H]_{i,j}, \quad (9)$$

where $[M/H]_{i,j}$ is a measure of the metallicity of the Cepheid, $[P]_{i,j} \equiv \log P_{i,j} - 1$ where $P_{i,j}$ is the period measured in days, M_H^W the absolute Cepheid magnitude normalized to a period of $P = 10$ days and Solar metallicity and μ_i the distance modulus to the i th galaxy. In what follows, we will allow for separate P-L relations for short and long period Cepheids using

$$b_W[P]_{i,j} \rightarrow b_W^s[P]_{i,j}^s + b_W^l[P]_{i,j}^l, \quad (10)$$

where $[P]_{i,j}^s = 0$ for Cepheids with periods > 10 days and $[P]_{i,j}^l = 0$ for Cepheids with periods < 10 days, see Section A.

Similarly for the j th Cepheid in the k th anchor galaxy, here MW, NGC 4258 and the Large Magellanic Cloud (LMC),

$$m_{H,k,j}^W = \mu_k + m_H^W + b_W[P]_{k,j} + Z_W[M/H]_{k,j}. \quad (11)$$

4.2. Milky Way Cepheids

Trigonometric parallaxes potentially provide the most direct calibration of the Cepheid absolute magnitude, M_H^W . We use data from Riess et al. (2021), with 75 MW Cepheids, out of which 68 have reliable GAIA parallaxes. For the j th Cepheid in the MW,

$$m_{H,j}^W = \mu_j + M_H^W + b_W[P]_j + Z_W[M/H]_j. \quad (12)$$

where the distance moduli for each Cepheid is estimated using GAIA parallaxes, π , according to

$$\pi_j + zp = 10^{-0.2(\mu_j - 10)}, \quad (13)$$

where zp is a residual parallax calibration offset that we fit for together with M_H^W , b_W and Z_W . In Riess et al. (2021), M_H^W and zp are fit for using only MW data setting $b_W = -3.26$ and $Z_W = -0.17$ (as fitted to all Cepheids), finding $zp = -14 \pm 6 \mu\text{as}$. Since we want to fit for zp simultaneously with all parameter, we write

$$\begin{aligned} \mu_j &= 10 - \frac{5}{\ln 10} \left[\ln \pi + \ln \left(1 + \frac{zp}{\pi} \right) \right] \\ &= 10 - \frac{5}{\ln 10} \left[\ln \pi + \frac{zp}{\pi} + \mathcal{O} \left(\frac{zp}{\pi} \right)^2 \right], \end{aligned} \quad (14)$$

effectively transforming zp into a linear parameter, and

$$\begin{aligned} m_{H,j}^W - 10 + \frac{5}{\ln 10} \ln \pi &= m_H^W + b_W[P]_j \\ &+ Z_W[M/H]_j - \frac{5}{\ln 10} \frac{zp}{\pi}. \end{aligned} \quad (15)$$

Higher order terms, $\mathcal{O}(zp/\pi)^2$, are small and corrected for in an iterative manner.

4.3. Type Ia Supernovae

The calibrated SNIa B-band peak magnitude in the i th host is modelled by

$$m_{B,i} = \mu_i + M_B. \quad (16)$$

The SNIa peak apparent magnitudes need to be corrected for the width-luminosity and C-L relations. There are several lightcurve fitting algorithms for deriving the SNIa peak magnitude, lightcurve shape and color, the most widely used for cosmology being the SALT2 model (Guy et al. 2007). The derived lightcurve widths and colors are used to correct the peak magnitude m_B in equation 16. The errors on the corrected peak magnitude include the fitting error and a 0.1 mag term from the SNIa model added in quadrature.

4.4. Data

For the extra-galactic (M31 and beyond) Cepheids, including Cepheids in the anchor galaxy NGC 4258, we use the data set from Table 4 in Riess et al. (2016). This table is restricted to Cepheids passing a best-fit, global 2.7σ outlier rejection, the impact of which is claimed to be small in Riess et al. (2016), but not possible to confirm independently by us.

For Cepheids in the LMC, we use data in Table 2 in Riess et al. (2019). Data for MW Cepheids, including GAIA parallax measurements are from Table 1 in Riess et al. (2021).

Double eclipsing binaries (DEBs) provide a means to measure distances by determining the physical sizes of the member stars via their radial velocities and light curves (Paczynski 1996). 20 DEBs observed using long-baseline near-infrared interferometry give a distance to the LMC of $\mu_{\text{LMC}} = 18.477 \pm 0.0263$ (Pietrzyński et al. 2019; Riess et al. 2019). We use the updated distance to NGC 4258 of $\mu_{\text{LMC}} = 29.397 \pm 0.032$ (Reid et al. 2019), using observations of mega-masers in Keplerian motion around its central super massive black hole.

Type Ia SN B-band magnitudes are from Table 5 in Riess et al. (2016), derived using version 2.4 of SALT II (Betoule et al. 2014).

4.5. Parameter Fitting

Given the observed Cepheid magnitudes m_H , colors $V-I$, periods $[P]$, metallicities $[M/H]$, together with the SNIa magnitudes m_B , the anchor distances μ_k and the MW Cepheid parallaxes π , we can fit simultaneously for R_W or R_E , b_W , Z_W , the host galaxy distances μ_i , the anchor distances μ_k , the GAIA parallax offset zp , the Cepheid absolute magnitude M_H^W and the SNIa absolute magnitude M_B . Since the system of equations is linear, the fit can be made analytically as described in Section A.

Given M_B , the Hubble constant is calculated as

$$H_0 = 10^{M_B/5+a_B+5} \quad (17)$$

where a_B is the intercept of the SNIa magnitude-redshift relation

$$10^{a_B+m_B/5} = cz \left\{ 1 + \frac{1}{2} [1 - q_0] z - \frac{1}{6} [1 - q_0 - 3q_0^2 + j_0] z^2 + O(z^3) \right\} \quad (18)$$

measured with $q_0 = -0.55$ and $j_0 = 1$ to $a_B = 0.71273 \pm 0.00176$ (Riess et al. 2016).

5. RESULTS FOR THE WESENHEIT CALIBRATION $R_W(V-I)$

In Riess et al. (2021), a value of $H_0 = 73.2 \pm 1.3$ is derived combing anchor distances from the MW, NGC 4258 and LMC.

Using the same data with $R_W = 0.386$, using double P-L relations, doing a full count-rate non-linearity correction following Riess et al. (2019), identifying $[O/H] = [Fe/H]$ using $Z_\odot = 8.824$, and fitting for the residual GAIA offset zp simultaneously with all other parameters, we obtain $H_0 = 73.1 \pm 1.3$. Here, we have added a scatter in the P-L relation of $\sigma(m_H^W) = 0.0682$, to give a $\chi^2/\text{dof} = 1$. Despite slight differences in the analysis method, this value is in very good agreement with the value in Riess et al. (2021), and in 4.1σ tension with the Planck value of $H_0 = 67.4 \pm 0.5$ (Aghanim et al. 2020).

5.1. Systematic Shift of R_W

The inferred value of H_0 will shift if there is a systematic offset in R_W between anchor and SNIa host galaxies. We derive values for H_0 when varying the value of R_W in the anchor(s) and the SNIa hosts, see Figure 3. For a common R_W (indicated by the dotted line), the inferred value of H_0 decreases when R_W is increased. Also, H_0 is decreased when R_W is larger in anchor than in host galaxies. Given the result in Figure 3, one could argue that a simple solution to the Hubble tension, would be a systematic shift of R_W between anchor and host galaxies of $\Delta R_W \sim 0.15$, bringing H_0 as inferred from SNIa

down to the Planck value. This could be argued for, e.g., if dust properties in SNIa host galaxies have a systematically steeper extinction law than the anchor galaxies. In lack of solid independent evidence for such a systematic shift, or the value of R_W and possible variations of it, we will next include R_W as a model parameter to be constrained by the available data.

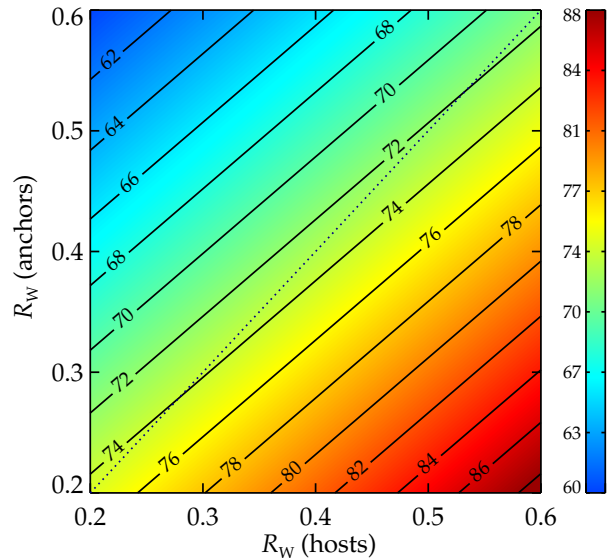


Figure 3. H_0 as a function of R_W , as used in the Wesenheit calibration with respect to $R_W(V-I)$, in SNIa hosts and anchor galaxies.

5.2. Fitting for R_W

The fact that dust extinction extrapolated to the H-band is very uncertain naturally opens up for the option of fitting for the value of R_W , either a global value common for all galaxies or individually for all galaxies. The first option gives $R_W = 0.31 \pm 0.02$ with $H_0 = 73.7 \pm 1.3$ with Planck tension 4.4σ .

If we allow for R_W to vary between galaxies we obtain the result in Figure 4, with host galaxies systematically favoring lower values for R_W , and $H_0 = 66.9 \pm 2.5$ in agreement with the Planck value. With a prior constraint on the individual values of R_W , centered on $R_W = 0.386$, the inferred H_0 will transition smoothly from $H_0 = 66.7 \pm 2.7$ (for an infinite prior width) to $H_0 = 73.1 \pm 1.3$ (for zero prior width). Imposing weak prior constraints of $R_W = 0.45 \pm 0.35$, guided by the discussion in Section 2, we obtain $H_0 = 69.4 \pm 2.6$ with Planck tension $< 1\sigma$.

5.3. Individual P-L relations

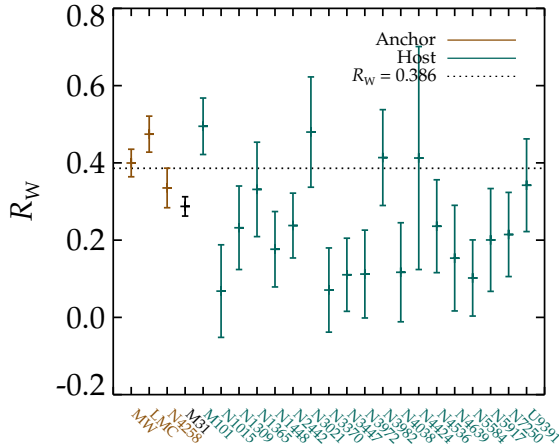


Figure 4. Fitting individual luminosity-color relations R_W ($V-I$) to Cepheid data. Anchor galaxies are denoted in brown and SNIa host galaxies in petrol. The dotted line corresponds to $R_W = 0.386$ as commonly assumed for Cepheid calibration.

So far, we have assumed that all Cepheids can be described by a global P-L relation, described by b_W^s and b_W^l . However, since there is evidence that the P-L relation can vary between galaxies (Tammann et al. 2011; Efsthathiou 2020), in a similar spirit to our approach of allowing R_W to vary between galaxies, we investigate to what extent relaxing this assumption will affect the inferred Hubble constant. We will allow for individual galactic values of $b_{W,i}$ to be fitted for simultaneously with all other parameters, in this case restricting to the same P-L relation for short and long period Cepheids. For a fixed global value of $R_W = 0.386$, the resulting $b_{W,i}$ are shown in Figure 5. The fact that the fitted $b_{W,i}$ are systematically higher in SNIa host galaxies compared to hosts, the inferred Hubble constant is increased from $H_0 = 73.1 \pm 1.3$ to $H_0 = 76.5 \pm 1.9$. If we allow for both individual P-L and C-L relations, the result is again shifted down to $H_0 = 66.1 \pm 2.7$.

6. RESULTS FOR COLOR EXCESS CALIBRATION

$R_E \hat{E}(V-I)$

We next compare with results derived when color calibrating the Cepheid sample with respect to the estimated color excess. We derive $\hat{E}(V-I)$ subtracting mean intrinsic colors as estimated in Tammann et al. (2011), including the quoted uncertainties and a 0.075 dispersion in the mean intrinsic Cepheid color between galaxies (inferred from the difference between LMC and MW Cepheids). These colors are in good agreement with results in Pejcha & Kochanek (2012). The intrinsic color uncertainties are included generating random

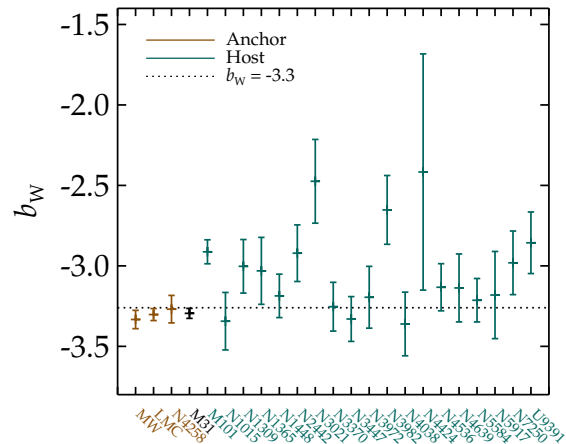


Figure 5. Fitting individual P-L relations b_W to Cepheid data. Anchor galaxies are denoted in brown and SNIa host galaxies in petrol. The dotted line corresponds to $b_W = -3.26$, indicating the value obtained assuming a global P-L relation.

Monte Carlo samples. The mean color excess range from $\hat{E}(V-I) = 0.28$ in the LMC to $\hat{E}(V-I) = 0.69$ in the MW, see also Figure 10. Calibrating using $R_E \hat{E}(V-I)$, for a fixed value of $R_E = 0.386$, we obtain $H_0 = 73.0 \pm 1.3$, showing the insensitivity of calibration method for fix values of R_W and R_E .

The derived value of H_0 depends on the assumed value for R_E in the anchor(s) and the SNIa hosts as depicted in Figure 6. We note a weaker dependence on the values of R_E when compared to the sensitivity of H_0 to R_W in the Wesenheit calibration, as shown in Figure 3.

6.1. Fitting for R_E

Fitting for a global value of R_E , common for all galaxies, gives $R_E = 0.31 \pm 0.02$ with $H_0 = 73.6 \pm 1.3$ increasing the Planck tension to 4.4σ .

We next allow for R_E to vary between galaxies. Since R_E represents a combination of corrections to both dust and intrinsic colors, both with large uncertainties in the NIR, we only impose weak prior constraints on their values $R_E = 0.45 \pm 0.35$ motivated by observations presented in Section 2, obtaining $H_0 = 71.8 \pm 1.6$ km/s/Mpc, in 2.7σ tension with the Planck value, see Figure 7. The priors keep the 1σ upper limit of the fitted values well within $R_E > 0$. Comparing with the results for R_W in Figure 4, it is evident that we get very similar results for R_E with increased error bars. The one exception is LMC for which the preferred value for R_E is significantly larger than for R_W . Not imposing any priors on R_E yields $H_0 = 70.9 \pm 1.7$ km/s/Mpc, in which case for N3370 only the 2σ upper limit has $R_E > 0$.

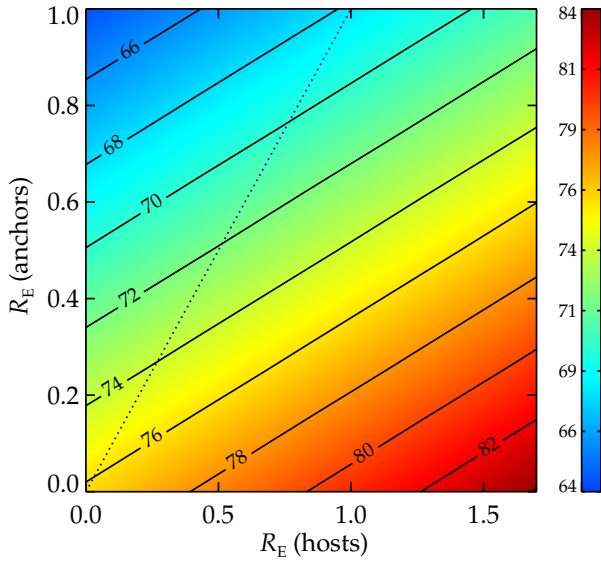


Figure 6. H_0 as a function of R_E in the SNIa hosts and the anchor galaxies when color calibrating Cepheids with respect to the estimated color excess $R_E \hat{E}(V - I)$.

Allowing also for individual galactic P-L relations, we obtain $H_0 = 73.5 \pm 2.0$ (3.0σ tension), assuming priors on R_E .

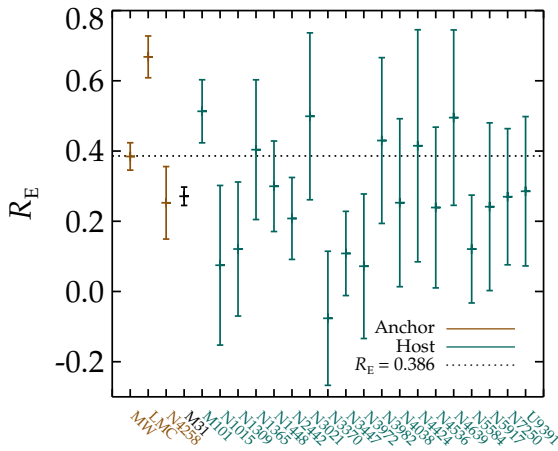


Figure 7. The result of fitting individual galactic values for R_E using the color excess Cepheid calibration, imposing prior constraints $R_E = 0.45 \pm 0.35$. Anchor galaxies are denoted in brown and SNIa host galaxies in petrol. The dotted line corresponds to $R_E = 0.386$.

7. SUMMARY AND DISCUSSION

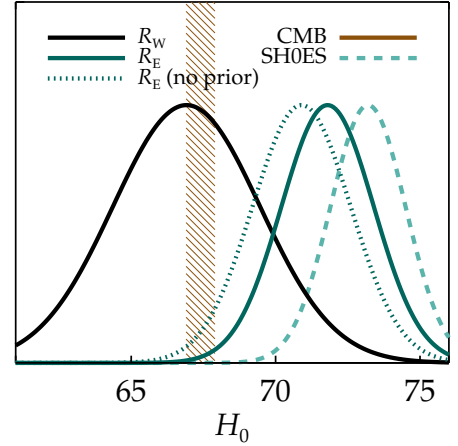


Figure 8. Results for H_0 for the two main analyses employed in this paper. The solid black line is for individual galactic values of R_W using Wesenheit magnitudes. The dark petrol lines are for individual R_E using color excesses, with the solid line assuming prior values $R_E = 0.45 \pm 0.35$. The dashed petrol line is fitted using the Wesenheit calibration with $R_W = 0.386$ as in Riess et al. (2021) and the dashed brown region indicates the 1σ region from Planck (Aghanim et al. 2020).

We have argued that the value inferred for the Hubble constant from SNIa distance measurements is quite sensitive to the choice of Cepheid calibration method. Specifically, we have compared results when color calibrating the Cepheid magnitudes with respect to observed colors and estimated color excesses. In both cases, guided by the lack of evidence for global dust extinction properties at NIR wavelengths, we have allowed for individual color calibrations in each galaxy. Regardless of whether we calibrate with respect to observed colors or estimated color excesses, the correction terms $R_W(V - I)$ and $R_E \hat{E}(V - I)$ only have clear interpretations if $\{R_W, R_E\} = R_H^{VI} = \beta_H^{VI}$, correcting for both dust extinction and intrinsic color variations. Both approaches could thus be regarded as partly phenomenological, and partly as a physical model parameterization.

For the color excess calibration, we derive $H_0 = 71.8 \pm 1.6$ in 2.7σ tension with the value inferred from Planck when using a weak prior of $R_E = 0.45 \pm 0.35$. With no prior, $H_0 = 70.9 \pm 1.7$ (2.0σ tension). Calibrating with respect to observed colors yields $H_0 = 66.9 \pm 2.5$ in agreement with the Planck value, see Figure 8. These results are stable to the possibility of also allowing for individual galactic P-L relations. Results for individual anchors are presented in Section C. The lower H_0 compared to the case of a fixed global color calibration is driven by the preferred lower values of R_W and R_E in

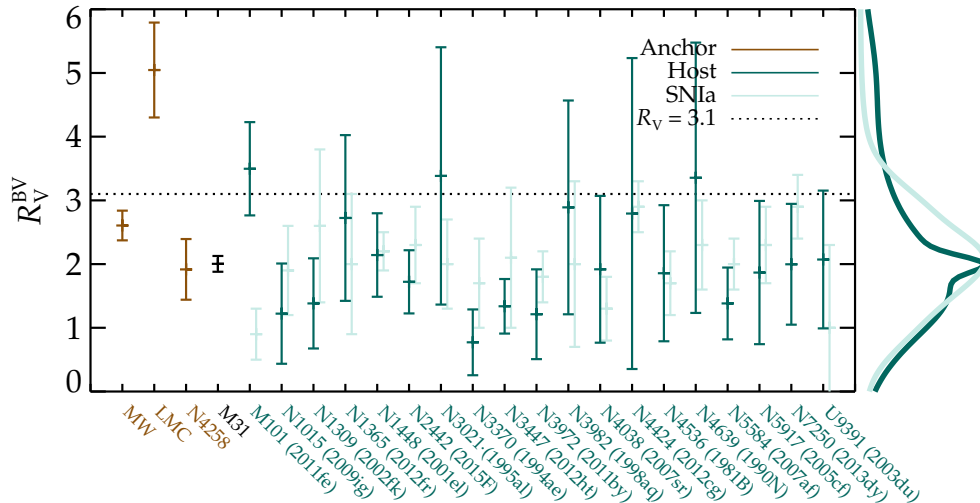


Figure 9. Comparing results for R_V^{BV} as fitted using the color excess Cepheid calibration (dark petrol) and independently from SNIa colors in Burns et al. (2018) (light petrol). The dotted line corresponds to $R_V^{BV} = 3.1$. Shown to the right of the plot are the total probability distribution functions for R_V^{BV} for the SNIa hosts, as derived from Cepheid and SNIa colors, respectively.

SNIa hosts. Comparing the SNIa host dust properties as inferred here from Cepheid data using color excesses with independent constraints from the SNIa color data from Burns et al. (2018) (derived using the CCM parameterization in Cardelli et al. 1989) shows a reassuring agreement, see Figure 9, with the one exception of SNIa 2011fe in M101.

Results for different calibration choices are summarized in Table 1 in Section B. From the quality of the fits, there is no clear preference for any of the calibration methods.

Regardless of calibration method, since Cepheid colors and periods are correlated (Tammann et al. 2011), so will the inferred P-L and C-L relations, i.e., the parameters b_W and R_W or R_E . This may be of importance if there are color selection effects related to the fact that longer period Cepheids are brighter, see Figure 10. We have tested the possible impact of such an effect by imposing cuts on the observed color $V-I$. In Figure 11, we show the fitted H_0 as a function of the cut in $(V-I)$ we apply, when calibrating using color excesses for a fixed $R_E = 0.386$. The trend of obtaining a lower H_0 when cutting out redder Cepheid is a common feature for all calibration methods we have tested.

Finally, we note that when estimating distances using the I-band for which color corrections are larger, unsurprisingly, the sensitivity of the result to the choice of calibration method is even larger. For example, with the Wesenheit calibration, assuming a fixed value of $R_{W,I}^{VI} = 1.27$ (corresponding to $R_H^{VI} = 0.386$), we obtain $H_0 = 70.4 \pm 1.5$, in 1.9σ tension with the CMB value, whereas allowing for individual galactic values of $R_{W,I}^{VI}$

yields $H_0 = 57.3 \pm 2.7$, in 3.7σ tension with Planck. With the color excess calibration, for $R_{E,I}^{VI} = 1.27$, we obtain $H_0 = 69.6 \pm 1.5$, in 1.4σ tension with the CMB value, whereas allowing for individual galactic values of $R_{E,I}^{VI}$ yields $H_0 = 66.9 \pm 1.3$, in agreement with Planck.

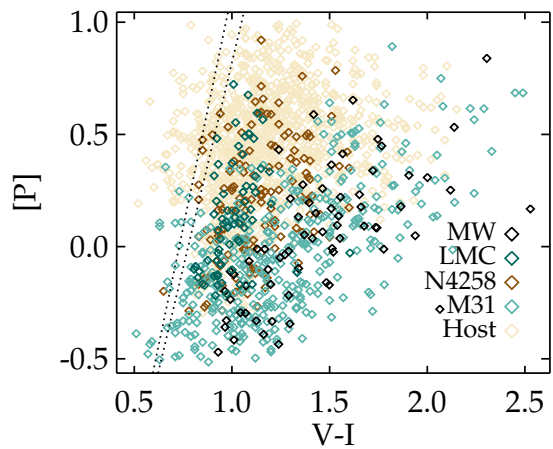


Figure 10. Observed Cepheid colors $V-I$ versus the periods $[P] = \log P - 1$. The dotted lines correspond to the upper and lower limit of the mean intrinsic MW Cepheid color as estimated in Tammann et al. (2011).

With the limited information at hand regarding dust extinction and intrinsic C-L relations for Cepheids at NIR wavelengths, and our current inability to distinguish between them in most cases, the color calibration of Cepheid magnitudes introduces large uncertainties in the local distance ladder. Neither approach employed in

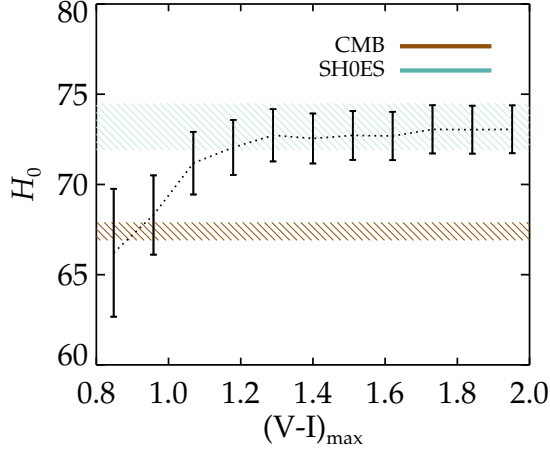


Figure 11. Fitted H_0 as a function of the cut in $(V - I)$ for a fixed value of $R_E = 0.386$ when calibrating using estimated color excesses.

this paper is in one-to-one correspondence with an underlying physical model and there is no clear evidence in the data for any of them. Given that results differ by $\delta H_0 \sim 5$, similar to the difference between the SH0Es and the Planck value and exceeding individual statistical errors by a factor $\gtrsim 2$, we conclude that systematic uncertainties related to the choice of Cepheid color-luminosity calibration method have the potential to resolve the current Hubble tension.

- 1 EM acknowledges support from the Swedish Research
- 2 Council under Dnr VR 2020-03384. AG acknowledges
- 3 support from the Swedish Research Council under Dnr
- 4 VR 2020-03444, and the Swedish National Space Board,
- 5 grant 110-18.

APPENDIX

A. SYSTEM OF EQUATIONS

Following [Riess et al. \(2016\)](#), we collect all data points and their corresponding uncertainties and possible correlations in the matrices \mathbf{Y} and \mathbf{C} . This includes the Wesenheit magnitudes of all Cepheids, $m_{H,i,j}^W$, including the anchors. The exception is the Milky Way Cepheids for which we use $m_{\pi,j} \equiv m_{H,j}^W - 10 + \frac{5}{\ln 10} \ln \pi$. Next, we have the measured anchor distances, μ_{N4258} , μ_{LMC} and possibly μ_{M31} . Finally, data points include the B-band SNIa magnitudes in the Cepheid hosts, $m_{B,i}$:

$$\mathbf{Y} = \begin{bmatrix} m_{\pi,j} \\ m_{H,1,j}^W \\ \vdots \\ m_{H,19,j}^W \\ m_{H,N4258,j}^W \\ m_{H,LMC,j}^W \\ \mu_{N4258} \\ \mu_{LMC} \\ m_{B,1} \\ \vdots \\ m_{B,19} \end{bmatrix}, \quad \mathbf{C} = \begin{bmatrix} \sigma^2(m_{\pi,j}) & 0 & \dots & & & & & & & 0 \\ 0 & \sigma^2(m_H^W) & 0 & \dots & & & & & & \vdots \\ \vdots & & \ddots & & & & & & & \\ & & & \sigma^2(\mu_{N4258}) & & & & & & \\ & & & & \sigma^2(\mu_{LMC}) & & & & & \\ & & & & & \sigma^2(m_{B,1}) & & & & \\ & & & & & & \ddots & & & \\ 0 & & & & & & & & & \sigma^2(m_{B,19}) \end{bmatrix} \quad (\text{A1})$$

Collecting the model parameters in the matrix \mathbf{X}

$$\mathbf{X} = \begin{bmatrix} \mu_{0,1} \\ \vdots \\ \mu_{0,19} \\ \mu_{\text{N4258}} \\ \mu_{\text{LMC}} \\ m_{\text{H}}^{\text{W}} \\ b_{\text{W}}^{\text{s}} \\ b_{\text{W}}^{\text{l}} \\ Z_{\text{W}} \\ zp \\ M_{\text{B}} \end{bmatrix}, \quad (\text{A2})$$

we can relate data and parameters through $\mathbf{Y} = \mathbf{A}\mathbf{X}$ where in schematic form

$$\mathbf{A} = \begin{bmatrix} 0 & \dots & & & 1 & [\text{P}]_{\text{MW},1}^{\text{s}} & [\text{P}]_{\text{MW},1}^{\text{l}} & [\text{M}/\text{H}]_1 & \frac{-5\pi_1^{-1}}{\ln 10} & 0 \\ \vdots & & & & & & & & & \\ 0 & & & & 1 & [\text{P}]_{\text{MW},N}^{\text{s}} & [\text{P}]_{\text{MW},N}^{\text{l}} & [\text{M}/\text{H}]_N & \frac{-5\pi_N^{-1}}{\ln 10} & 0 \\ 1 & 0 & \dots & & 1 & [\text{P}]^{\text{s}} & [\text{P}]^{\text{l}} & [\text{M}/\text{H}] & 0 & \vdots \\ \vdots & 1 & 0 & \dots & 1 & \vdots & \vdots & \vdots & \vdots & \vdots \\ & \dots & & & 1 & 0 & 0 & & & \\ & & & & & 1 & 0 & & & \\ 1 & 0 & \dots & & & & & & & 1 \\ 0 & 1 & 0 & \dots & & & & & & 1 \\ \vdots & & & & & & & & & \vdots \\ 0 & \dots & & & 1 & 0 & \dots & & & 1 \end{bmatrix}. \quad (\text{A3})$$

Note that the first N rows correspond to equation 15 and so forth, so that \mathbf{A} is a $n_{\text{param}} \times n_{\text{data}}$ matrix. We can solve for the parameter matrix \mathbf{X} and its covariance matrix Σ analytically

$$\Sigma = [\mathbf{A}^T \mathbf{C}^{-1} \mathbf{A}]^{-1}, \quad \mathbf{X} = \Sigma [\mathbf{A}^T \mathbf{C}^{-1} \mathbf{Y}]. \quad (\text{A4})$$

Note that the formalism can easily extended to fit also for, e.g., R_{W} and R_{E} , and that parameter priors are incorporated as additional data points.

B. MODEL SELECTION

The choice of C-L and P-L calibration method can have a large impact on the inferred H_0 . Unfortunately, from data alone, it is not obvious which of calibration models is preferred. Specifically, there is no clear preference in data for color calibrating with respect to observed colors or estimated color excesses. As expected, allowing for more freedom in the model, the fit will improve². In terms of model selection, results are ambiguous, see Table 1. Here, the Akaike Information Criterion (AIC) and the Bayesian Information Criterion (BIC) are defined by

$$\begin{aligned} \text{AIC} &\equiv 2n_{\text{par}} + \chi^2, \\ \text{BIC} &\equiv n_{\text{par}} \ln n_{\text{dat}} + \chi^2, \end{aligned} \quad (\text{B5})$$

² When comparing the quality of the fit for different models, we add the same additional scatter to the P-L relation. When constraining parameters within a given model, the scatter is adjusted to give a $\chi^2/\text{dof} = 1$.

Table 1. Resulting H_0 and quality of fit for different color calibration models for Wesenheit calibration, R_W ($V - I$), and color excess calibration, $R_E \hat{E}(V - I)$. The prior for the color excess calibration refer to $R_E = 0.45 \pm 0.35$.

Wesenheit cal.	H_0 (Planck tension)	χ^2_{\min}	AIC	BIC
$R_W = 0.386$	73.1 ± 1.3 (4.1σ)	1616.6	1672.6	1823.9
Global R_W	73.7 ± 1.3 (4.4σ)	1602.4	1660.4	1817.1
Individual R_W	66.9 ± 2.5 (0.2σ)	1549.2	1651.2	1926.9
Individual b_W	76.5 ± 1.9 (4.5σ)	1566.0	1664.0	1928.9
Individual R_W and b_W	66.4 ± 2.8 (0.4σ)	1497.4	1641.4	2030.6
Color excess cal.	H_0 (Planck tension)	χ^2_{\min}	AIC	BIC
$R_E = 0.386$	73.0 ± 1.3 (4.0σ)	1612.7	1668.7	1820.0
Global R_E	73.6 ± 1.3 (4.4σ)	1598.9	1656.9	1813.7
Individual R_E (w prior)	71.8 ± 1.6 (2.7σ)	1610.2	1712.2	1988.6
Individual R_E (wo prior)	70.9 ± 1.7 (2.0σ)	1533.9	1635.9	1911.6
Individual b_W	76.1 ± 1.9 (4.4σ)	1563.5	1661.5	1926.3
Individual R_E and b_W (w prior)	73.5 ± 2.0 (3.0σ)	1504.8	1648.8	2039.0
Individual R_E and b_W (wo prior)	72.4 ± 1.9 (2.5σ)	1487.0	1631.0	2020.2

with the latter more penalizing for models with extra parameters for $n_{\text{dat}} > 8$. In terms of the AIC, fitting for individual values of R_W or R_E and b_W is the preferred model, whereas in terms of BIC, a global fitted value yields the best result. As it stands, it is unclear to what degree these results provide guidance on the choice of calibration model.

C. RESULTS FOR INDIVIDUAL ANCHORS

In Figure 12, we show the inferred Hubble constant from each individual anchor. Here, we have used individually fitted R_W and R_E for each galaxy but assumed a global P-L relation. Also allowing for b_W to vary between galaxies yields similar results. Dotted lines are for a global value $R_W = 0.386$ using the Wesenheit calibration, closest resembling the case in Riess et al. (2021). The solid lines are for the case of fitting for individual R_W and R_E . The main difference in both cases, besides broadening the likelihoods, is the shift of LMC anchor result.

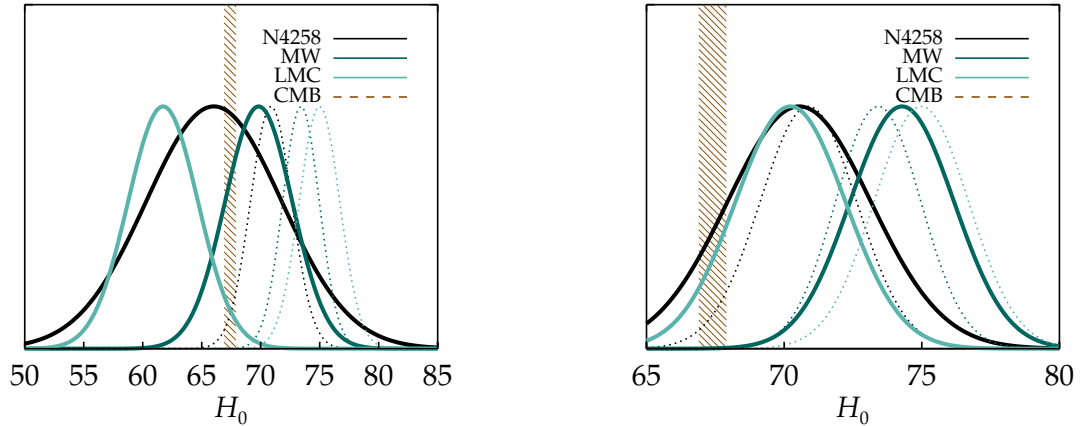


Figure 12. Results for H_0 for different anchor distances. Dotted lines are fitted using the Wesenheit calibration with $R_W = 0.386$ as in Riess et al. (2021). *Left panel:* Solid lines are fitted for individual galactic values of R_W using Wesenheit magnitudes. *Right panel:* Solid lines are fitted for individual galactic values of R_E using estimated color excesses.

REFERENCES

- Abbott, B. P., et al. 2017, Nature, 551, 85, doi: 10.1038/nature24471
- Aghanim, N., Akrami, Y., Ashdown, M., et al. 2020, A&A, 641, A6, doi: 10.1051/0004-6361/201833910

- Amanullah, R., Goobar, A., Johansson, J., et al. 2014, *ApJL*, 788, L21, doi: [10.1088/2041-8205/788/2/L21](https://doi.org/10.1088/2041-8205/788/2/L21)
- Amanullah, R., Johansson, J., Goobar, A., et al. 2015, *MNRAS*, 453, 3300, doi: [10.1093/mnras/stv1505](https://doi.org/10.1093/mnras/stv1505)
- Betoule, M., Kessler, R., Guy, J., et al. 2014, *A&A*, 568, A22, doi: [10.1051/0004-6361/201423413](https://doi.org/10.1051/0004-6361/201423413)
- Birrer, S., Shajib, A. J., Galan, A., et al. 2020, *A&A*, 643, A165, doi: [10.1051/0004-6361/202038861](https://doi.org/10.1051/0004-6361/202038861)
- Biswas, R., Goobar, A., Dhawan, S., et al. 2021, arXiv e-prints, arXiv:2103.16978.
<https://arxiv.org/abs/2103.16978>
- Brout, D., & Scolnic, D. 2021, *ApJ*, 909, 26, doi: [10.3847/1538-4357/abd69b](https://doi.org/10.3847/1538-4357/abd69b)
- Burns, C. R., Parent, E., Phillips, M. M., et al. 2018, *ApJ*, 869, 56, doi: [10.3847/1538-4357/aae51c](https://doi.org/10.3847/1538-4357/aae51c)
- Burns, C. R., et al. 2018, *ApJ*, 869, 56, doi: [10.3847/1538-4357/aae51c](https://doi.org/10.3847/1538-4357/aae51c)
- Cardelli, J. A., Clayton, G. C., & Mathis, J. S. 1989, *ApJ*, 345, 245, doi: [10.1086/167900](https://doi.org/10.1086/167900)
- Dhawan, S., Brout, D., Scolnic, D., et al. 2020, *ApJ*, 894, 54, doi: [10.3847/1538-4357/ab7fb0](https://doi.org/10.3847/1538-4357/ab7fb0)
- Draine, B. T. 2003, *ARA&A*, 41, 241, doi: [10.1146/annurev.astro.41.011802.094840](https://doi.org/10.1146/annurev.astro.41.011802.094840)
- Efstathiou, G. 2020, A Lockdown Perspective on the Hubble Tension (with comments from the SH0ES team).
<https://arxiv.org/abs/2007.10716>
- Fausnaugh, M. M., Kochanek, C. S., Gerke, J. R., et al. 2015, *MNRAS*, 450, 3597, doi: [10.1093/mnras/stv881](https://doi.org/10.1093/mnras/stv881)
- Fitzpatrick, E. L. 1999, *PASP*, 111, 63, doi: [10.1086/316293](https://doi.org/10.1086/316293)
- Fitzpatrick, E. L., Massa, D., Gordon, K. D., Bohlin, R., & Clayton, G. C. 2019, *ApJ*, 886, 108, doi: [10.3847/1538-4357/ab4c3a](https://doi.org/10.3847/1538-4357/ab4c3a)
- Follin, B., & Knox, L. 2018, *MNRAS*, 477, 4534–4542, doi: [10.1093/mnras/sty720](https://doi.org/10.1093/mnras/sty720)
- Freedman, W. L., Madore, B. F., Hatt, D., et al. 2019, *ApJ*, 882, 34, doi: [10.3847/1538-4357/ab2f73](https://doi.org/10.3847/1538-4357/ab2f73)
- Goobar, A., Johansson, J., Amanullah, R., et al. 2014, *ApJL*, 784, L12, doi: [10.1088/2041-8205/784/1/L12](https://doi.org/10.1088/2041-8205/784/1/L12)
- Gordon, K. D., Clayton, G. C., Misselt, K. A., Landolt, A. U., & Wolff, M. J. 2003, *ApJ*, 594, 279, doi: [10.1086/376774](https://doi.org/10.1086/376774)
- Guy, J., Astier, P., Baumont, S., et al. 2007, *A&A*, 466, 11, doi: [10.1051/0004-6361:20066930](https://doi.org/10.1051/0004-6361:20066930)
- Johansson, J., Cenko, S. B., Fox, O. D., et al. 2021, arXiv e-prints, arXiv:2105.06236.
<https://arxiv.org/abs/2105.06236>
- Knox, L., & Millea, M. 2020, *PhRvD*, 101, doi: [10.1103/physrevd.101.043533](https://doi.org/10.1103/physrevd.101.043533)
- Krisciunas, K., Prieto, J. L., Garnavich, P. M., et al. 2006, *AJ*, 131, 1639, doi: [10.1086/499523](https://doi.org/10.1086/499523)
- Madore, B. F. 1982, *ApJ*, 253, 575, doi: [10.1086/159659](https://doi.org/10.1086/159659)
- Madore, B. F., Freedman, W. L., & Moak, S. 2017, *ApJ*, 842, 42, doi: [10.3847/1538-4357/aa6e4d](https://doi.org/10.3847/1538-4357/aa6e4d)
- Mörtsell, E., & Dhawan, S. 2018, *JCAP*, 2018, 025–025, doi: [10.1088/1475-7516/2018/09/025](https://doi.org/10.1088/1475-7516/2018/09/025)
- Nataf, D. M., Gonzalez, O. A., Casagrande, L., et al. 2016, *MNRAS*, 456, 2692, doi: [10.1093/mnras/stv2843](https://doi.org/10.1093/mnras/stv2843)
- Nobili, S., & Goobar, A. 2008, *A&A*, 487, 19, doi: [10.1051/0004-6361:20079292](https://doi.org/10.1051/0004-6361:20079292)
- O'Donnell, J. E. 1994, *ApJ*, 422, 158, doi: [10.1086/173713](https://doi.org/10.1086/173713)
- Paczynski, B. 1996.
<https://arxiv.org/abs/astro-ph/9608094>
- Pejcha, O., & Kochanek, C. S. 2012, *ApJ*, 748, 107, doi: [10.1088/0004-637x/748/2/107](https://doi.org/10.1088/0004-637x/748/2/107)
- Pietrzyński, G., Graczyk, D., Galle, A., et al. 2019, *Nature*, 567, 200–203, doi: [10.1038/s41586-019-0999-4](https://doi.org/10.1038/s41586-019-0999-4)
- Reid, M. J., Pesce, D. W., & Riess, A. G. 2019, *ApJ*, 886, L27, doi: [10.3847/2041-8213/ab552d](https://doi.org/10.3847/2041-8213/ab552d)
- Riess, A. G., Casertano, S., Yuan, W., et al. 2021, *ApJ*, 908, L6, doi: [10.3847/2041-8213/abdbaf](https://doi.org/10.3847/2041-8213/abdbaf)
- Riess, A. G., Casertano, S., Yuan, W., Macri, L. M., & Scolnic, D. 2019, *ApJ*, 876, 85, doi: [10.3847/1538-4357/ab1422](https://doi.org/10.3847/1538-4357/ab1422)
- Riess, A. G., Narayan, G., & Calamida, A. 2019, Calibration of the WFC3-IR Count-rate Nonlinearity, Sub-percent Accuracy for a Factor of a Million in Flux, Space Telescope WFC Instrument Science Report
- Riess, A. G., et al. 2016, *ApJ*, 826, 56, doi: [10.3847/0004-637X/826/1/56](https://doi.org/10.3847/0004-637X/826/1/56)
- Rigault, M., Brinnel, V., Aldering, G., et al. 2020, *A&A*, 644, A176, doi: [10.1051/0004-6361/201730404](https://doi.org/10.1051/0004-6361/201730404)
- Schlafly, E. F., Peek, J. E. G., Finkbeiner, D. P., & Green, G. M. 2017, *ApJ*, 838, 36, doi: [10.3847/1538-4357/aa619d](https://doi.org/10.3847/1538-4357/aa619d)
- Tammann, G. A., Reindl, B., & Sandage, A. 2011, *A&A*, 531, A134, doi: [10.1051/0004-6361/201016382](https://doi.org/10.1051/0004-6361/201016382)

This figure "orcid-ID.png" is available in "png" format from:

<http://arxiv.org/ps/2105.11461v1>